Overcharged lipid metabolism in mechanisms of antitumor by *Tremella fuciformis*-derived polysaccharide

XIUMIN LI*, QIAOLING SU* and YUTIAN PAN

The Engineering Technological Center of Mushroom Industry, Minnan Normal University, Zhangzhou, Fujian 363000, P.R. China

Received September 21, 2022; Accepted November 9, 2022

DOI: 10.3892/ijo.2022.5459

Abstract. *Tremella fuciformis*-derived polysaccharide (TFP) is a natural macromolecular compound that is well known for whitening skin, as well as for its ability to regulate lipids and immunity. However, its mechanism of action is not clear. In the present study, B16 cells treated with TFP were inoculated subcutaneously in the right flank of C57BL/6 mice to explore the effect of TFP on melanoma *in vivo*. Western blotting, immunohistochemistry, immunofluorescence staining and transcription analysis of tumors were utilized to assess the expression of key molecules in production of melanin, lipid metabolism and immunity. It was found that TFP promoted B16 cell apoptosis and induced G_2/M cell cycle arrest, which was associated with activation of cell cycle-related pathways. TFP induced the expression of glucose transporter type 4 and CD36, thus resulting in an increase in the uptake of lipids, which markedly suppressed sterol regulatory element-binding transcription factor 1 and phosphorylated-AMP-activated protein kinase expression; increased the number of lipids in the cell membrane, endoplasmic reticulum and nucleus; and induced the RNA expression of molecules related to lipid metabolism, as revealed by RNA-sequencing *in vivo*. Increased lipid binding, upregulated lipid storage, and elevated triglyceride and lipid catabolism resulted in disruption of cell volume homeostasis and activated innate immune response, thus inhibiting melanoma development and progression. These data revealed a novel molecular mechanism involved in the antitumor effect of TFP via lipid metabolism.

Correspondence to: Dr Xiumin Li or Professor Yutian Pan, The Engineering Technological Center of Mushroom Industry, Minnan Normal University, 36 Xianqianzhi Road, Zhangzhou, Fujian 363000, P.R. China
E-mail: lixiumins06@163.com
E-mail: xmpyt@sina.com; pyt1106@mnnu.edu.cn

*Contributed equally

Abbreviations: TFP, *Tremella fuciformis*-derived polysaccharides; SREBP, sterol regulatory element binding protein; ER, endoplasmic reticulum; ACLY, ATP-citrate lyase; ACC, acetyl CoA carboxylase; FAS, fatty acid synthase; GLUT4, glucose transport 4; PPARγ, peroxisome proliferator-activated receptor γ; RTCA, real time cellular analysis; DEGs, differentially expressed genes; GO, Gene Ontology; KEGG, Kyoto Encyclopedia of Genes and Genomes; GSEA, Gene Set Enrichment Analysis; SRA, Sequence Read Archive; AMPK, adenosine 5'-monophosphate-activated protein kinase; pAMPK, phosphorylated-AMP-activated protein kinase; GAPDH, glyceraldehyde-3-phosphate dehydrogenase; ANOVA, Analysis of Variance; LPL, lipoprotein lipase; Trarg1, trafficking regulator of GLUT4; TCA, tricarboxylic acid cycle; FA, fatty acid; WB, western blotting

Key words: *Tremella fuciformis*-derived polysaccharide, B16 cells, overcharged lipid metabolism

Introduction

Malignant melanoma is one of the most aggressive tumor types, and is characterized by high proliferation rates, poor prognosis and low survival rate (1). The high rate of metastasis is the main cause of mortality in patients with melanoma (2). Previous evidence has shown that altered tumor metabolism suppresses the infiltration of immune cells and helps melanoma cells to escape the immunity of the host (3).

Metabolic reprogramming is a hallmark of cancer (4), and a lipogenic phenotype is a main characteristic of cancer. Sterol regulatory element binding protein (SREBP) has been reported to be highly activated in tumors, and their levels and activity are tightly controlled by endogenous sterol levels via a negative feedback loop. Sterols regulate SREBP by controlling its endoplasmic reticulum (ER)-to-Golgi apparatus transport (5). SREBPs control lipogenesis and lipid uptake, SREBP1 preferentially regulates the lipogenic process by activating genes involved in fatty acid and triglyceride synthesis (6), whereas SREBP2 primarily controls cholesterol homeostasis by activating genes required for cholesterol synthesis and uptake (7).

Cancer cells become independent of systemic regulation due to their autonomous generation of lipids. Cancer cells engage in extensive *de novo* lipogenesis to produce lipids (8). Three important enzymes in *de novo* fatty acid synthesis, namely ATP-citrate lyase (ACLY), acetyl coenzyme A (CoA) carboxylase (ACC) and fatty acid synthase (FAS), are upregulated in numerous types of cancer (9). ACLY produces acetyl CoA, in the cytoplasm and provides the precursor of lipid synthesis, while ACC controls the rate-limiting step of fatty acid synthesis. FAS has been shown to play a key role in

tumor malignant growth and at the terminal step in *de novo* synthesis of fatty acids (10). The *FAS* and *ACC* genes are directly regulated by SREBP1 in fatty acid synthesis. ACLY involved in cholesterol synthesis also participates in fatty acid biosynthesis (11), and is required for glucose transporter type 4 (GLUT4)-mediated glucose-dependent fatty acid synthesis (12).

Cancer cells have alternative ways to acquire nutrients, and certain tumors develop adaptations that allow them to intake fatty acids directly from plasma or surrounding adipose tissue (13). Increasing lipid biosynthesis occurs in cancer cells, which influences the tumor microenvironment, and SREBP1 transcription factors respond to diverse environmental changes, such as lipid supply and inflammatory signals (14). Cells deal with excess lipids such as fatty acids by esterifying them to form more inert neutral lipids, such as triacylglycerols or sterol esters. Peroxisome proliferator-activated receptor γ (PPARγ) plays a major role in adipogenesis and storage of fatty acids such as triglycerides (15). The formation of these neutral lipids occurs within membrane bilayers; however, since bilayers are not suitable for storing large quantities of neutral lipids, an emulsion of neutral-lipid droplets forms in the cytoplasm (16). Lipid trafficking is highly organized and regulated in space. The aforementioned neutral-lipid emulsion originates in the ER, which serves as a phospholipid reservoir in cells to generate stable emulsions (17). When ER emulsions are delayed, this leads to accumulation of neutral lipids in the ER and blebbing out into inappropriate sites such as the nucleus (18). Lipids in the nucleus can sequester transcription factors and chromatin components, as well as generate lipoid ligands for certain nuclear receptors (17).

Tremella fuciformis-derived polysaccharide (TFP) is extracted from *Tremella fuciformis*, which is a common nutritional food in China and also a traditional Chinese medicine due to its anti-inflammatory and anticancer properties, and its ability to strengthen immunity, and reduce hypertension and blood glucose (19). TFP has also been used clinically for whitening skin, cancer and anti-aging treatments in China. However, the protective mechanism of TFP is not clear yet. The present study explored the function of TFP on the lipid metabolism of B16 cells, and evaluated lipid metabolism changes influenced the tumor growth and microenvironment *in vivo*.

Materials and methods

Cell culture and treatment. The B16 mouse melanoma cells line was purchased from the cell bank of Chinese Academy of Sciences (Shanghai, China). Cells were cultured in DMEM medium with phenol red, supplemented with 10% FBS, 100 U/ml penicillin, and 100 μg/ml streptomycin in a dynamic incubation system at 37˚C in a 5%-CO_2 humidified atmosphere. The cells were treated in the presence of series of dosages of TFP (0, 312.5, 625, 1,250, 2,500 and 5,000 μg/ml) for 24 h.

HPLC analysis of TFP. The content of TFP in B16 cells was detected by high-performance lipid chromatography (HPLC). Briefly, the B16 cells with or without TFP exposure were centrifuged at 1,000 x g for 3 min at room temperature and suspended with ultrapure water in ice bath for 10 min, then centrifuged for 10 min. The supernatant was collected for HPLC. HPLC separation was performed on sugar column (water ultra-hydrogel 500) and detected using differential detector 1200 (Agilent Technologies, Inc.). The mobile phase was ultrapure water. The column temperature was kept at 85˚C and the flow rate was set at 0.6 ml/min.

Animal model and drug treatment. A total of 18 male C57BL/6 mice (6-8 weeks old; weight, 25 g) were purchased from Shanghai Experimental Animal Center, Chinese Academy of Sciences (Shanghai, China). The mice were housed in temperature (25˚C) and humidity (30-40%)-controlled room, kept on a 12-h light/dark cycle and provided with unrestricted amount of rodent chow and water. The animal protocol was approved (approval no. 2020002) by the Animal Care and Use Committee of Minnan Normal University (Zhangzhou, China).

To study the direct effects of TFP *in vivo* tumor development, B16 cells were preincubated *in vitro* with two dosages of TFP (2,500 and 5,000 μg/ml). After 24 h, the cells were washed 3 times, and $1x10^6$ B16 cells/ml resuspended in 100 μl of PBS were inoculated subcutaneously in the right flank of the mice. The tumor volume 2,000 mm^3 calculated according to length and width was a limit or the maximum permitted tumour burden in the present study. At the experiment terminal, the mice were sacrificed by cervical dislocation, sacrifice was confirmed when the mice had ceased breathing and did not respond to stimulation. The tumors were collected and weight was measured.

Cell proliferation assay. For determination of cell growth using Real Time Cellular Analysis (RTCA), plate 16 assemblies were seeded with B16 cells ($1x10^4$ cells/well). The plate was then assembled on the RTCA DP analyzer, after 24 h cells were treated with five dosages of TFP (312.5, 625, 1,250, 2,500, 5,000 μg/ml), and data were gathered at 5-min intervals for 120 h at 37˚C in 5% CO_2.

Flow cytometric analysis of cell cycle, apoptosis and co-localization. Cells were harvested by treatment with 0.25% trypsin, resuspended with PBS, then stained with propidium iodide and Annexin V. (cat. no. C1062M′ Beyotime Institute of Biotechnology) in dark at room temperature for 10-20 min; DNA content of the cells was stained by DAPI at room temperature for 5 min. For co-localization, cells were stained with Cytopainter Golgi/ER staining κit (cat. no. ab139485; Abcam), the Golgi should exhibit green fluorescence, and ER should fluoresce red. Cell membrane was stained by Dio fluoresce green (cat. no. C1993S; Beyotime Institute of Biotechnology). Imaging flow cytometry (EMD Millipore) was adjusted according to the procedure previously described (20). Acquisition speed was set up to low speed and the highest resolution. Cells were acquired based on area and aspect ratio, gating out single cells from the analysis. A total number of 10,000 cells for each sample were acquired. Channel 2 was used to acquire Annexin V or Golgi, cell membrane signaling, channel 4 was used to detect Nile red, channel 7 was used to detect DAPI and channel 5 was used to detect propidium iodide or ER. Data were analyzed in IDEAS 6.2 software (EMD Millipore) after compensation of single-color control samples using a compensation matrix. Co-localization of

membrane, ER, Golgi, or nucleus with lipid was analyzed using colocalization analysis application Wizard in IDEAS software.

Nile Red staining. B16 cells cultured on confocal dish (Coverglass Bottom Dish) were treated with different concentrations of TFP for 24 h. Then the cells were stained by Nile red (1:500) and DAPI (1:1,000) for 30 min avoiding light, and then images were captured using confocal laser scanning microscope (Leica Microsystems GmbH).

Western blotting (WB). The protein levels and phosphorylation status were examined by WB. The cells were washed twice with ice-cold PBS and lysed in RIPA protein lysis buffer containing 1 mM PMSF (cat. no. R0010′ Beijing Solarbio Science & Technology Co., Ltd.). The samples were centrifuged at 13,000 x g for 10 min at 4˚C before the supernatant was collected and the protein concentration was measured using a BCA kit (cat. no. P0012; Beyotime Institute of Biotechnology). Samples were boiled for 5 min after being mixed with a 5X loading buffer solution. The protein lysates (30 μg) were resolved in 8-10% SDS-polyacrylamide gels and transferred to nitrocellulose membranes. The membranes were blocked using 5% skimmed milk for 1 h at room temperature, washed three times with TBST (0.1% Tween 20) for 10 min and then incubated overnight at 4˚C with various primary antibodies: anti-Adenosine 5'-monophosphate-activated protein kinase (AMPK; 1:2,000; cat. no. ab32047; Abcam), anti-phosphorylated-AMP-activated protein kinase (p-AMPK, 1:2,000; cat. no. EPR3051; Abcam), anti-SREBP-2 (1:500; cat. no. ab30682; Abcam), anti-PPARγ (1:1,000; cat. no. C26H12; Cell Signaling Technology, Inc.), anti-ACLY (1:1,000; cat. no. ab40793; Abcam), anti- Lysosomal-associated membrane protein1 (LAMP1; 1:1,000; cat. no. ab24170; Abcam), anti-CD36 (1:5,000; cat. no. ab133625; Abcam), anti-GLUT4 (1:500; cat. no. ab33780; Abcam), anti-p-GLUT4 (1:2,000; cat. no. ab188317; Abcam), anti-FAS (1:5,000; cat. no. ab128870; Abcam), anti-ACC (1:1,000; cat. no. EP687Y; Abcam), anti-SREBP1 (1:1,000; cat. no. NB600-582; Novus Biologicals, LLC). After incubation with rabbit HRP-conjugated secondary antibody (1:8,000; cat. no. HAF008; R&D Systems, Inc.) or mouse HRP-conjugated secondary antibody (1:8,000; cat. no. HAF007; R&D Systems, Inc.), the immunoreactivity was detected with using ECL solution (Beijing Solarbio Science & Technology Co., Ltd.). Bands were scanned by OmegaLum C image system (Aplegen, Inc.). Band signals were corrected by the Tubulin (1:1,000; cat. no. NB600-936; Novus Biologicals, Inc.) or glyceraldehyde-3-phosphate dehydrogenase (GAPDH; 1:2,000; cat. no. ab9485; Abcam) signals.

Hematoxylin and eosin (H&E) staining. Paraffin-embedded sections were cut at 3 μm thickness, mounted on microslides and processed for H&E staining, as previously described (21). The stained slides were dehydrated and mounted using Cytoseal. Images of the slides were captured (magnification, x200) with a light microscope (Olympus Corporation).

Immunohistochemistry. For immunohistochemistry, tissue sections were deparaffinized with xylene and stepwise rehydrated with serial dilutions of ethanol. After epitope retrieval with citric acid buffer under high temperature and pressure for 1-2 min, and endogenous horseradish peroxidase activity quenching with 3% H_2O_2 for 10 min, the tissue sections were then blocked in 5% goat serum (cat. no. C0265; Beyotime Institute of Biotechnology) at room temperature for 1 h and incubated with rabbit anti-mouse (ACLY, 1:100; PPARγ, 1:100; LAMP1, 1:100), and mouse anti-mouse antibody (PDL1, 1:100, cat. no. ab238697; CD68, 1:100, cat. no. NB600-985; CD86, 1:50, cat. no. ab220188; all from Abcam) at 4˚C overnight. The primary antibody was visualized by using anti-rabbit Alexa Fluor 647 (1:1,000; cat. no. P0180; Beyotime Institute of Biotechnology), and anti-mouse FITC conjugated antibody (1:1,000; cat. no. P0196; Beyotime Institute of Biotechnology). The images were captured using Leica TCS SP8 confocal laser microscope.

RNA-seq, data processing, and gene annotation. RNA of Model group and 5,000 μg/ml TFP group were extracted. Total RNA was extracted using TRIzol reagent kit (Invitrogen; Thermo Fisher scientific, Inc.). RNA quality was assessed on an Agilent 2100 Bioanalyzer (Agilent Technologies, Inc.). After total RNA was extracted, mRNA was enriched by Oligo (dT) beads. Then the enriched mRNA was fragmented into short fragments using fragmentation buffer and reversely transcribed into cDNA by using NEBNext Ultra RNA Library Prep Kit for Illumina (New England Biolabs). The purified double-stranded cDNA fragments were end repaired, a base added, and ligated to Illumina sequencing adapters. The ligation reaction was purified, ligated fragments were subjected to size selection (200 bp) by AMPure XP Beads (1.0X) and PCR amplification. The resulting cDNA library was sequenced using Illumina Novaseq6000 by Gene De novo Biotechnology Co. (Guangzhou, China).

High quality clean reads were further filtered by fastp (version 0.18.0). The gene expression level was normalized by using Fragments Per Kilobase of transcript per Million mapped reads. The genes with a fold change ≥2 and $P<0.05$ were considered as significant differentially expressed genes (DEGs). Three samples were prepared from each treatment.

Gene Ontology (GO) enrichment of DEGs was performed, the significantly enriched GO terms in DEGs was performed by comparing to the genome background using hypergeometric test. The biological pathways of the DEGs were enriched to the Kyoto Encyclopedia of Genes and Genomes (KEGG) using hypergeometric test as the above GO term enrichment (https://www.genome.jp/kegg/). Gene Set Enrichment Analysis (GSEA) (22) was used to identify whether a set of genes in specific GO terms\KEGG pathways\Reactome pathways shows significant differences in two groups. The sequences data reported in the present study was archived in the Sequence Read Archive (SRA) with the accession number BioProject ID PRJNA772896 (https://www.ncbi.nlm.nih.gov/bioproject/PRJNA772896/).

Statistical analysis. The data was examined using the statistical analysis program SPSS 22.0 (IBM Corp.). The data are expressed as the mean ± SD. Tumors weight were analyzed by using one-way Analysis of Variance (ANOVA)

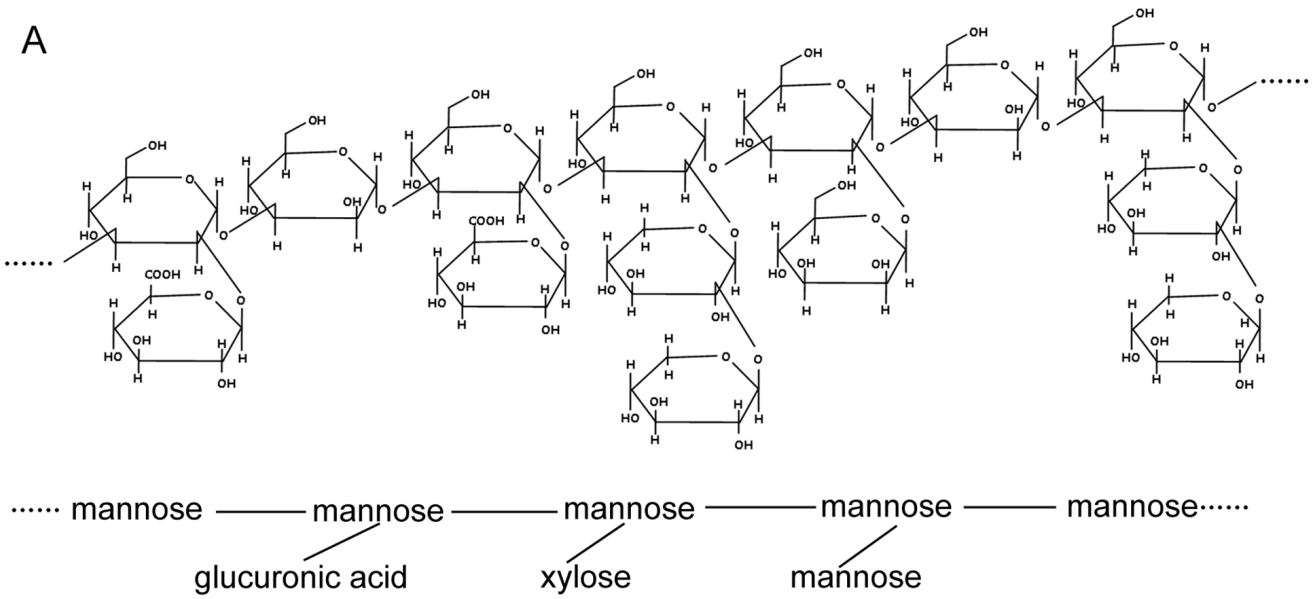

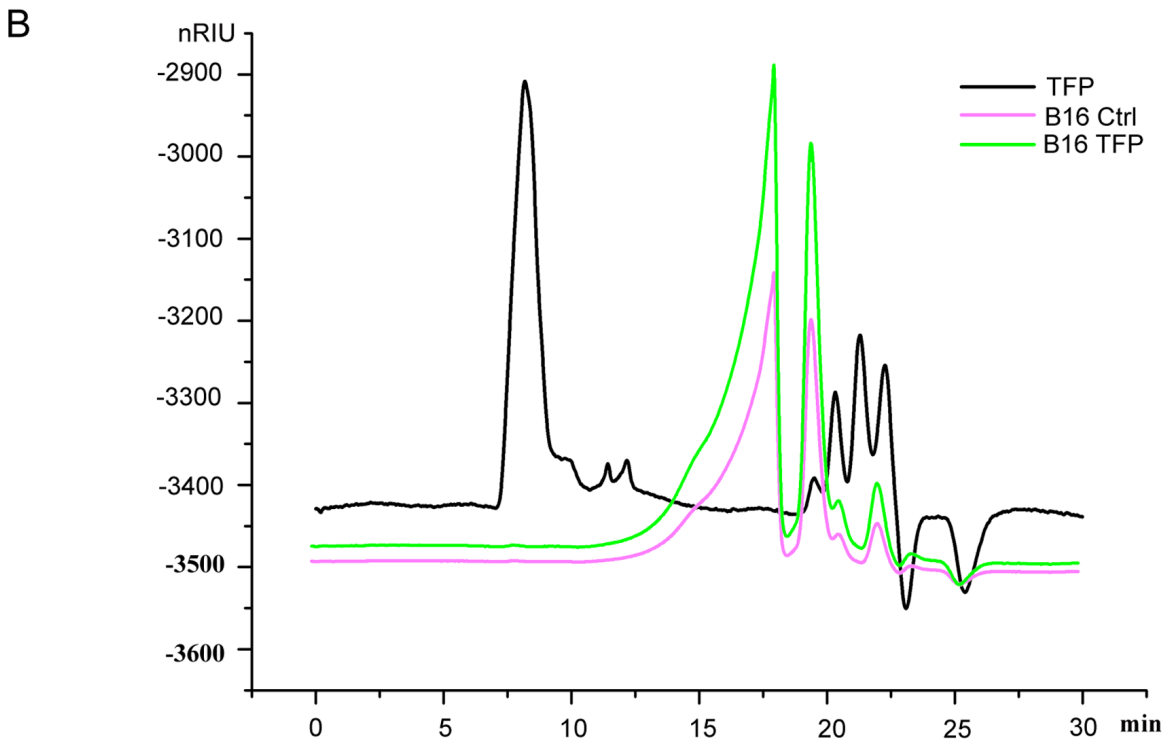

Figure 1. (A) Structure and (B) High-performance liquid chromatography analysis of TFP. TFP, *Tremella fuciformis*-derived polysaccharide.

followed by Fisher's least significant difference post hoc test for comparison between two groups. $P<0.05$ was considered to indicate a statistically significant difference.

Results

TFP structure and HPLC analysis. TFP is a polysaccharide whose main chain is mannan, which is a linear (1→3)-linked backbone, and its side chain is composed of mannose, glucuronic acid and xylose in uncertain order, as shown in Fig. 1A. The results of HPLC analysis results showed that there was no obvious TFP peak, since the TFP standard occurred at 8.183 min in B16 cells exposed to TFP, as shown in Fig. 1B. These data suggested that there was no TFP in B16 cells within the detection capability of HPLC.

Effects of TFP on anti-proliferation, pro-apoptosis and cell cycle arrest in vitro. The viability of B16 cells treated with TFP decreased in a dose-dependent manner, particularly at 1,250, 2,500 and 5,000 μg/ml TFP, which significantly inhibited the rate of B16 cell proliferation compared with the effects of other dosages of TFP (Fig. 2A). The effect of TFP on the relative proliferation rate of B16 cells was measured by its IC_{50}, which was calculated to be 1.836×10^7 μg/ml.

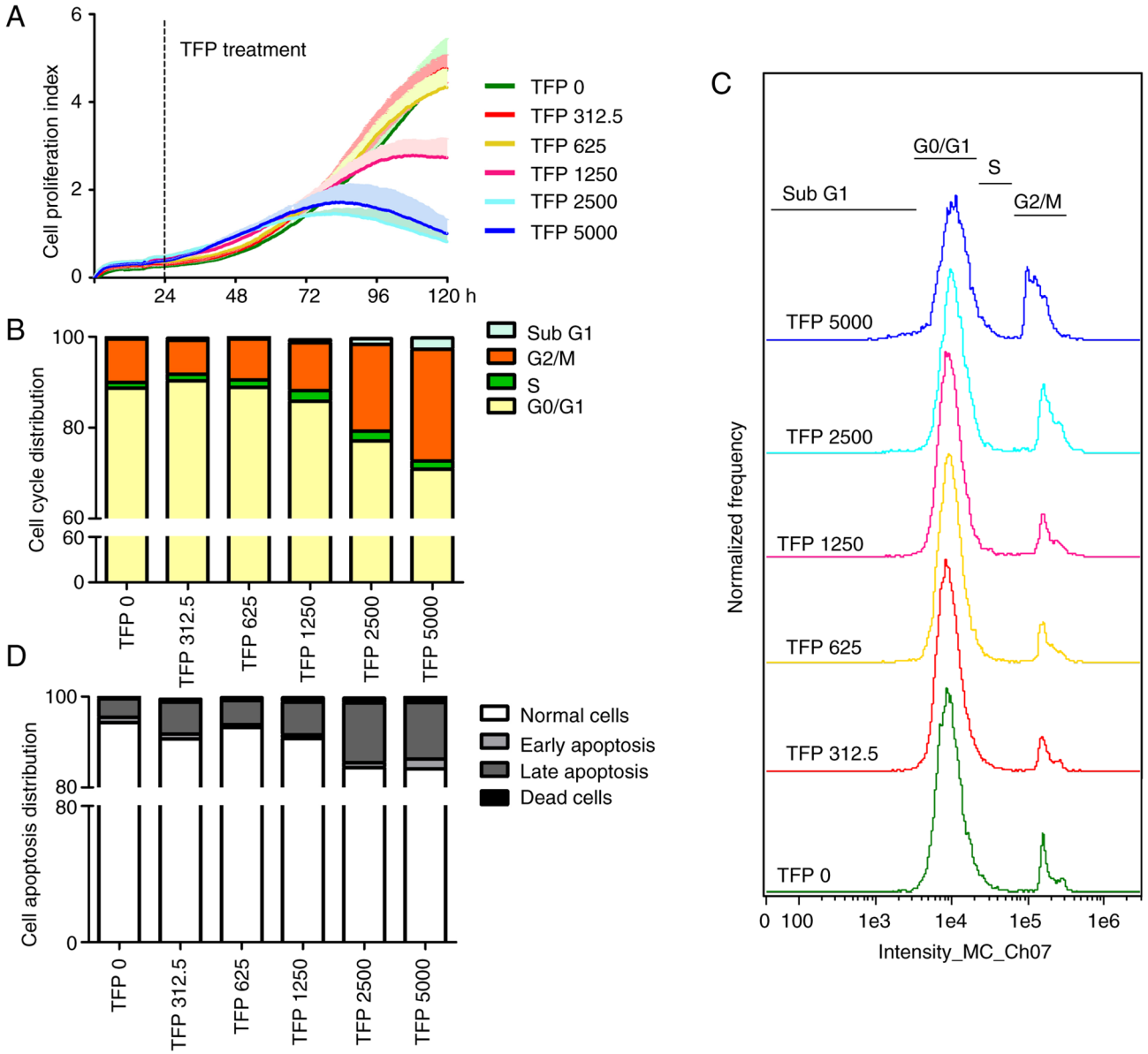

Figure 2. Effect of TFP on antiproliferation, pro-apoptosis and cell cycle arrest *in vitro*. (A) B16 cell proliferation curves. (B) Effect of TFP on cell cycle distribution. Flow cytometric analysis of (C) cell cycle and (D) cell apoptosis. TFP, *Tremella fuciformis*-derived polysaccharide.

To determine whether TFP inhibits B16 cell proliferation via cell cycle arrest, the DNA contents of the cells were measured by flow cytometry upon staining the cell nuclei with DAPI (Figs. 2B and C, and S1). The data showed that high dosages of TFP increased the number of cells in the G_2/M phase from 9.5% (0 μg/ml TFP) to 10.6% (1,250 μg/ml TFP), 19.1% (2,500 μg/ml TFP) and 24.6% (5,000 μg/ml TFP), while reducing the number of cells in the G_1 phase from 88.7% (0 μg/ml TFP) to 85.8% (1,250 μg/ml TFP), 77.1% (2,500 μg/ml TFP) and 70.9% (5,000 μg/ml TFP). In addition, TFP slightly increased the number of cells in S phase from 1.27% to 1.44, 1.58, 2.32, 2.17 or 1.73% depending on the concentration employed. These results suggested that TFP inhibited cell proliferation mainly by inducing G_2/M cell cycle arrest without cycle progression to G_1 phase through mitosis in B16 cells.

Flow cytometry was used to evaluate the state of cell apoptosis (Figs. 2D and S1). The results showed that the proportion of early apoptotic cells in untreated B16 cells was 1.13%, which slightly decreased with increasing concentration of TFP (312.5, 625, 1,250 and 2,500 μg/ml). When the concentration of TFP reached 5,000 μg/ml, 2.16% of cells were markedly early apoptotic cells. B16 cells exposed to 0, 312.5, 625, 1,250, 2,500 and 5,000 μg/ml of TFP for 24 h experienced an induction of 4.05, 7.02, 5.32, 7.19, 13.15, 12.40% in late apoptosis, respectively. In addition, the proportion of necrotic cells increased gradually with increasing concentrations of TFP. These data revealed that TFP at suitable concentrations could effectively induce B16 cell death following late apoptosis, rather than early apoptosis, and necrosis.

Lipids uptake reprograms lipogenesis profile in vitro. TFP markedly suppressed SREBP1 nuclear translocation, and suppressed SREBP1 target proteins, such as ACC and FAS, leading to reduced *de novo* lipogenesis (Fig. 3A). Unexpectedly, the ACLY and plasma lipids levels increased

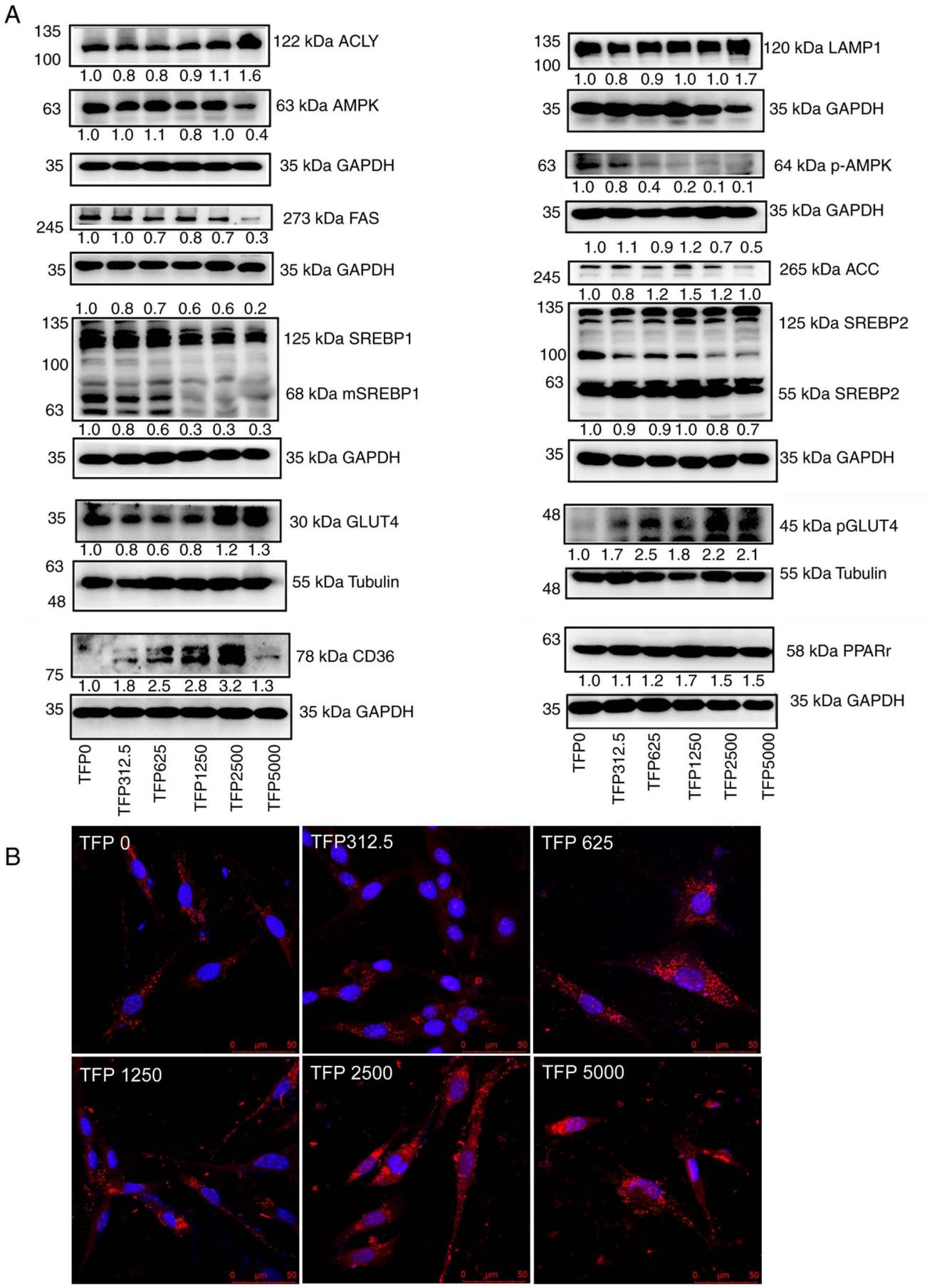

Figure 3. Uptake of exogenous lipids and reprogrammed lipogenesis profile *in vitro*. (A) The levels of lipogenesis-related protein were detected by western blotting. (B) Fluorescence analysis of lipids. SREBP, sterol regulatory element binding protein; GLUT4, glucose transport 4; ACC, Aacetyl CoA carboxylase; FAS, fatty acid synthase; ACLY, ATP-citrate lyase.

according to increasing TFP dosages (Fig. 3B). To explain why these apparent contradictions coexisted in B16 treated by TFP, the levels of GLUT4 and CD36 (lipid transport receptor) were analyzed, since cancer cells use glucose as well as fatty acids for ATP production, and GLUT4 and CD36 migrate together in response to either stimuli, i.e. glucose or fatty acids (23). The results confirmed that TFP induced high expression of GLUT4 and CD36 (Fig. 3A), which resulted in an increased uptake of exogenous lipids, which were present at higher lipid fluorescence intensity in the cell membrane (Fig. 4A; panels a and b) and plasma, including ER (Fig. 4B; panels a and b), nucleus (Fig. 4D; panels a and b) as compared with that of control group. However, the uptake of lipids present in the Golgi apparatus was decreased at dosage of TFP5000 (Fig. 4C; panels a and b). The aforementioned data was in accordance with higher co-localization ratios of lipids with the cellular membrane and nucleus (Fig. 4E), and higher lipid intensity of the whole cell compared with that of the vehicle group (Fig. 4F).

The intracellular accumulation of lipids, particularly in the ER, inhibited the maturation of SREBP1 and the expression of full-length SREBP1 (Fig. 3A). Lipids are important molecules in the nucleus, there is emerging evidence (24) for the existence of a nuclear population of lipids, which has been proposed to directly modulate lipid metabolism in the nucleus. In the present study, the lipids in the nucleus may have the functions of generating lipoid ligands for PPARγ, or cause chromosome segregation abnormalities, or modulate exogeneous lipid metabolism and storage.

TFP delays B16 allograft tumor growth and reduces tumor weight. Above results have shown that TFP induces the regulation of lipogenesis in B16 cells. To explore whether this response is capable of preventing or slowing tumor growth, $1x10^6$ B16 cells treated with or without TFP were subcutaneously injected in the right flank of C57 BL/6 mice (Fig. 5A). There were no significant differences in body weight of TFP treated groups referring to model group (Fig. 5B), while tumors grew more slowly and the tumor weights of the TFP-treated groups were less than those of B16 tumor-bearing mice (Fig. 5C). The tumor weights in the model and TFP 2,500 and 5,000 μg/ml groups were analyzed by one-way ANOVA followed by Fisher's least significant difference post hoc test (Fig. 5D), which revealed a significant difference among the three groups [$F(2,14)=13.595$, $P=0.001$]. The tumor weight of the TFP 2,500 μg/ml group exhibited a significant decrease compared with that of the model group ($P=0.007$), as well as the TFP 5,000 μg/ml group ($P=0.001$).

The histological characteristics were evaluated by (H&E) staining (Fig. 5E), which revealed increased pigmentation located in the model tumor section (as indicated by more white arrows), but less pigmentation (less white arrows) and scattered vacuoles in the TFP-treated tumor section (red arrows), which may be due to lipid accumulation, and was dissolved by xylene during H&E staining. These data suggested that TFP-treated B16 cells reprogrammed their lipid metabolism profile, and TFP promoted lipid accumulation in B16 cells.

WB analysis showed upregulation of ACLY and PPARγ (Fig. 5F and G). Upregulated ACLY and PPARγ activity increased lipid formation. As revealed by immunohistochemistry (Figs. 6A and S2), TFP upregulated the expression of ACLY and PPARγ, and promoted macrophage infiltration (as indicated by the increase in CD86 expression). Notably, LAMP1 expression increased according to the increase in TFP dosage. In certain areas of the TFP-treated groups, the formation of certain strip (long and linear) and round vacuoles was observed (the round vacuoles gathered at one end, while the strip vacuoles aligned orderly, similar to a 'balsam pear' surface), which was accompanied by the presence of numerous macrophages (Fig. 6B). Increased macrophage infiltration occurred when there was no formation of these structures. Not far from those structures, a number of bigger vacuoles could be observed, such as lipid accumulation dissolved by xylene in the process of staining, similar to the vacuoles noted during H&E staining (Fig. 5E). These data indicated that TFP controlled B16 allograft tumor growth through lipid metabolism regulation, and enhanced the antitumor immune response through macrophage infiltration and upregulation of LAMP1.

RNA-sequencing (RNA-seq) analysis of differentiated gene expression and enriched pathways. To further uncover the molecular mechanism of TFP, tumor gene expression profile analyses were conducted with the aim of uncovering valuable information for pharmacological research on therapeutic targets. Gene Ontology pathway enrichment analysis showed that negative regulation of mitotic cell cycle, regulation of cell proliferation and cell proliferation were significantly altered by TFP (Fig. 7A). The enrichment in pathways of cell cycle/proliferation confirmed the results of cell experiments.

Gene set enrichment analysis (GSEA) of the cell cycle-related RNA-seq results (Fig. 7B) showed that TFP treatment was strongly associated with the gene signature of cell cycle arrest, cell cycle and cycle phase transition. Furthermore, negative regulation of cell process, cell cycle and cell cycle phase transition were significantly positively associated with TFP. These data indicated that cell cycle regulation played an important role in the antitumor activity of TFP.

To determine whether the antitumor effect of TFP occurred through activation of lipid metabolism, gene expression was examined. Gene microarray analysis demonstrated the upregulation of mRNAs encoding genes involved in lipid metabolism (Fig. 8A), including glucolipid receptors (*CD36* and *Trarg1*: trafficking regulator of *GLUT4*), lipogenesis-related genes (*ACLY*), a set of mRNAs involved in the tricarboxylic acid cycle (Fig. 8B), and a number of lipolysis-related genes (such as *LPL*: lipoprotein lipase). GSEA of regulation of lipolysis in adipocytes further provided clues on the sources of lipids: upregulation of lipolysis of adipocyte in tumor indicated the possible sources of more lipids deposit in tumor (Fig. 8C). The omics effect of TFP on lipid metabolism is consistent with the aforementioned phenotypic results associated with increased lipid deposits in mitochondria, nucleus, ER and membrane, as well as the WB results related to increased glycolipid transport and increased lipid accumulation in allografts.

Subsequently, to identify the potential reason responsible for the activated lipid metabolism and to uncover the underlying molecular mechanisms of TFP involved in lipid metabolic processes, GSEA was used to mine the RNA-seq data. The results revealed that TFP treatment was associated

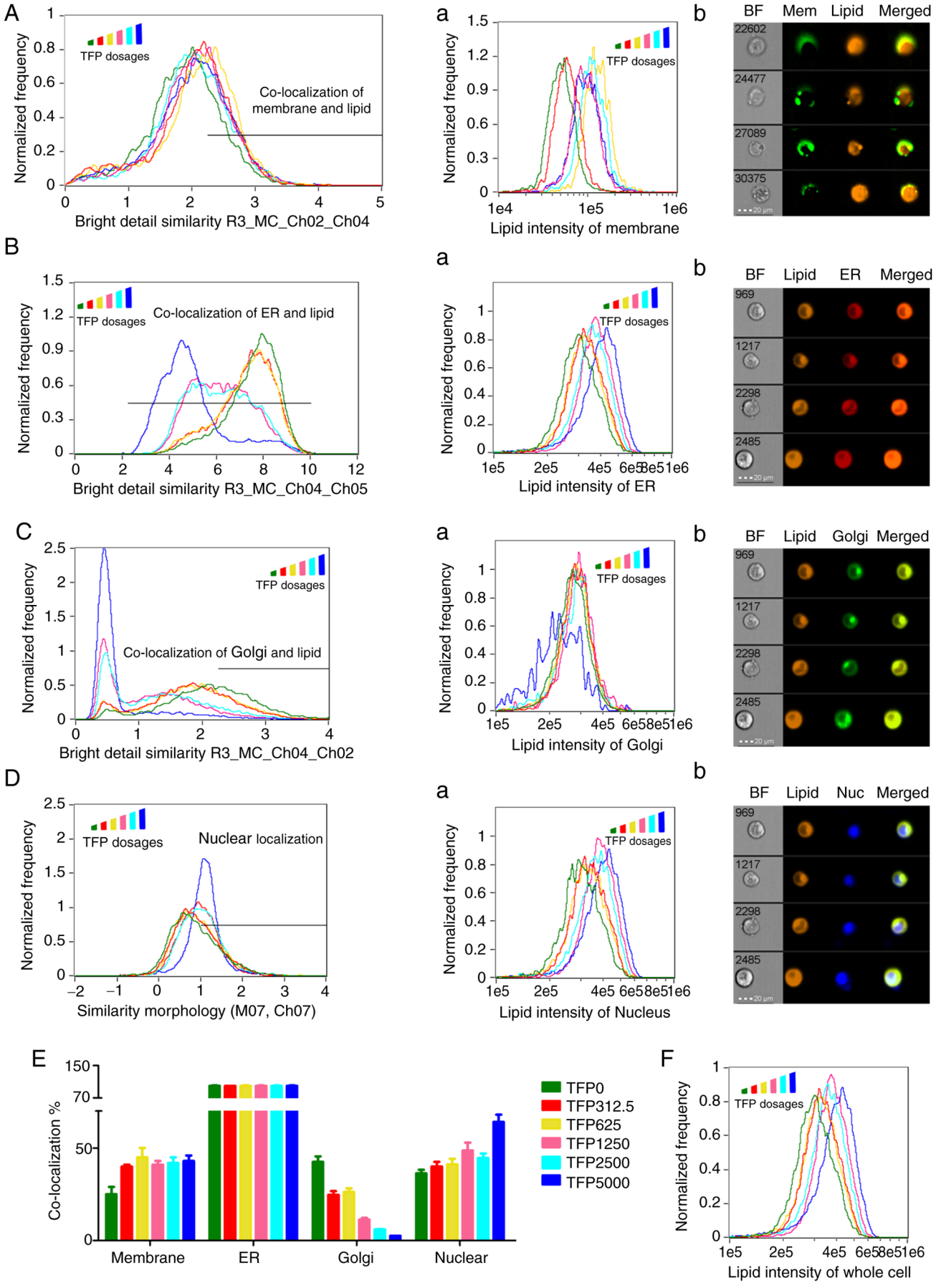

Figure 4. TFP regulates lipid distribution in B16 cells. Flow cytometric analysis of co-localization of lipids and (A) membrane, (B) ER, (C) Golgi apparatus, and (D) nucleus. Lipid intensity and representative images of (A panels a and b) membrane, (B panels a and b) ER, (C panels a and b) Golgi apparatus, and (D panels a and b) nucleus. (E) Statistical analysis of the results of panels A-D. (F) Lipid intensity of the whole cell. ER, endoplasmic reticulum; TFP, *Tremella fuciformis*-derived polysaccharide.

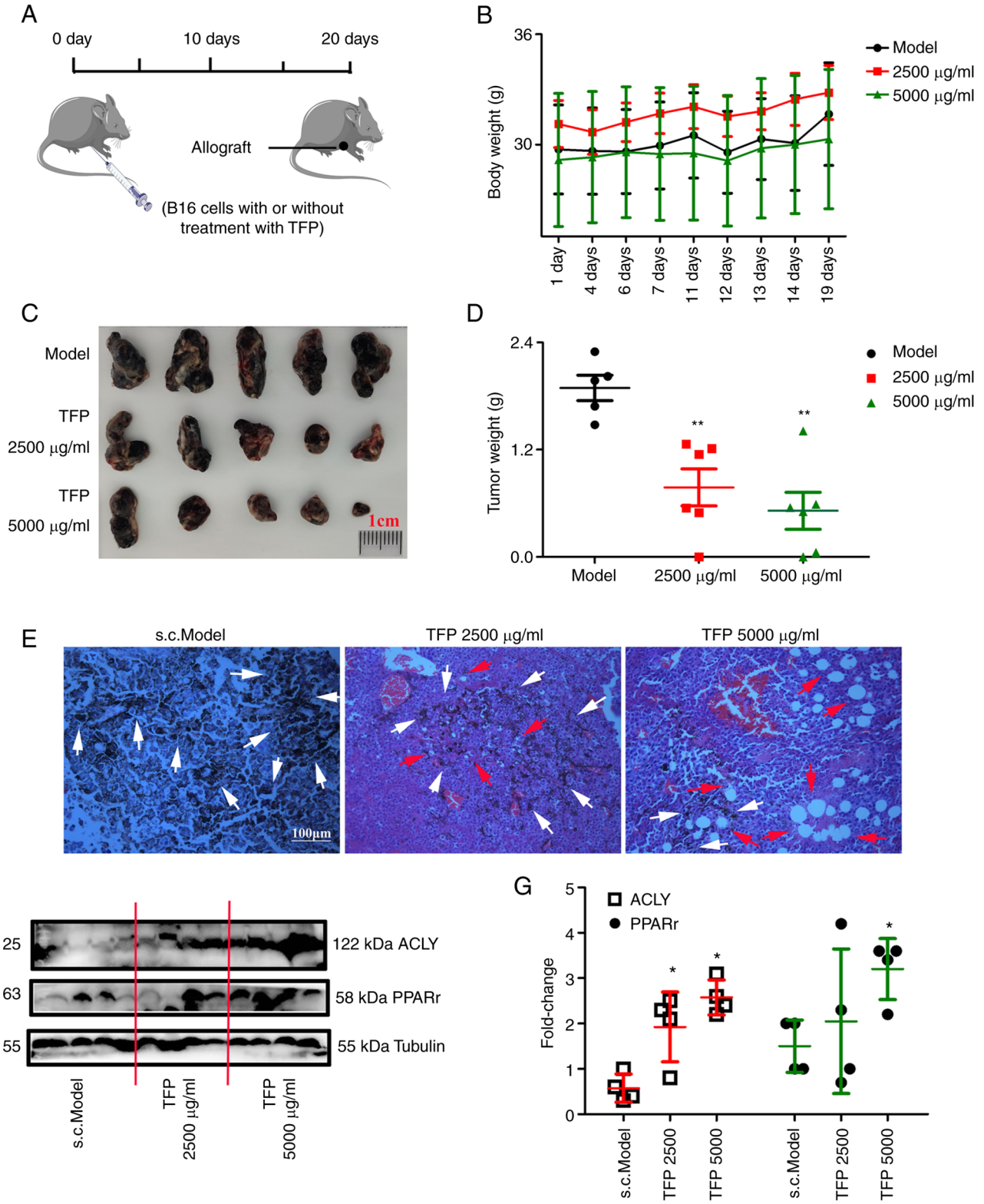

Figure 5. TFP delays B16 allograft tumor growth and reduces tumor weight. (A) Diagram of C57BL/6 mice inoculated subcutaneously with B16 cells. (B) The body weight of mice was recorded during the experimental period. (C) Subcutaneous tumors and (D) tumor weight at the end of the experiment. (E) The subcutaneous tumor sections were stained with hematoxylin and eosin. (F) The protein levels of ATP-citrate lyase and peroxisome proliferator-activated receptor γ were detected by western blotting. (G) Relative quantitative analysis of ATP-citrate lyase and peroxisome proliferator-activated receptor γ. TFP, *Tremella fuciformis*-derived polysaccharide; PPARγ, peroxisome proliferator-activated receptor γ; ACLY, ATP-citrate lyase.

with the gene signatures of 'positive regulation of lipid binding' (Fig. 9A), 'positive regulation of lipid storage' (Fig. 9B), 'triglyceride catabolism' (Fig. 9C) and 'lipid catabolism' (Fig. 9D). These results indicated that TFP not only promoted lipid uptake in cells, but also provoked lipid catabolism.

Next, it was hypothesized that metabolic changes could induce the immune system. It was found that TFP induced the enrichment

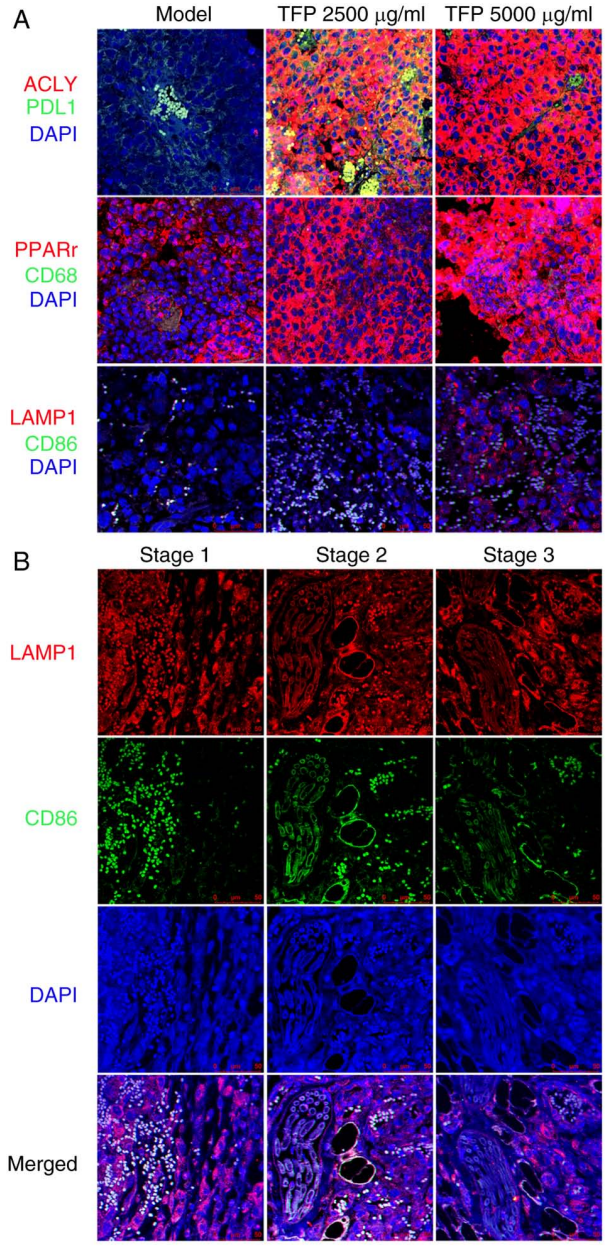

Figure 6. (A) TFP regulates ACLY and PPARγ expression, and promotes macrophage infiltration. Representative images of immunofluorescence staining of ACLY, PPARγ and lysosomal-associated membrane protein 1 (red); programmed cell death ligand 1, CD86 and CD68 (green); and DAPI (blue) (B). A 'balsam pear'-like structure was formed in the TFP treatment groups, which included round and strip vacuoles, and was accompanied by M1 macrophages. Increased macrophage infiltration occurred when these structures had not been formed yet. TFP, *Tremella fuciformis*-derived polysaccharide; ACLY, ATP-citrate lyase; PPARγ, peroxisome proliferator-activated receptor γ.

of gene transcription signatures of 'cell volume homeostasis' (Fig. 9E), 'response to reactive oxygen species' (Fig. 9F) and 'innate immune system' (Fig. 9G), thus activating the immune system (Fig. 9H). These results confirmed the mechanisms of TFP against B16 subcutaneous allografts, suggesting that TFP activated the immune system disrupting cell volume homeostasis.

Discussion

Regarding the initial step of the antitumor mechanism of TFP, it is worth noting that the high molecular weight of TFP greatly increases the viscosity of liquids, and the glucuronic acids in TFP have the ability to entrap cholesterol (25). These combined TFP with cell membrane or intercellular cholesterol were easily removed by centrifugation in the process of intracellular fluid extraction. This may explain why no TFP was detected in B16 cells by HPLC analysis. The receptors of TFP have not been identified to date. The antitumor mechanism of TFP may involve the upregulation of glucolipid receptors, such as CD36 and GLUT4, which were markedly elevated *in vitro* and *in vivo* in the present study.

The current study demonstrated the influence of TFP on the proliferation, cell cycle and apoptosis of B16 cells. TFP inhibited cell proliferation, induced cell apoptosis and altered cell cycle distribution. In addition, TFP downregulated SREBP, which regulates cellular lipogenesis and lipid homeostasis (26), and has been shown to be involved in other cellular functions, such as regulation of cell cycle and cell proliferation (27). TFP inhibited *de novo* lipogenesis through SREBP1, thereby inhibiting cell proliferation. TFP could prevent cells from completing mitosis, arresting them at a 'lipogenic' G_2/M phase. AMPK has been reported to exert anti-proliferative action (28). AMPK is a cell-intrinsic regulator of the cell cycle that coordinates cellular proliferation with energy source availability, and regulates a number of key cellular metabolic enzymes (29). The inhibitor effect of TFP on phosphorylated (p)-AMPK suggested that the anti-proliferative effect of TFP was AMPK independent. The nutrient sensor AMPK negatively regulates SREBP to limit lipogenesis under nutrient-limiting conditions (30). Cancer cell metabolism could be changed if sufficient ATP and the building blocks needed to sustain molecular synthesis were available. In the present study, the expression levels of AMPK and particularly those of p-AMPK were decreased by TFP, and AMPK positively regulated SREBP when CD36 and GLUT4 were notably upregulated by TFP. Loss of AMPK or downregulation of AMPK results in energy stress-driven apoptosis, and slows down tumor progression (31); AMPK inhibitors rather than activators could preferentially trigger cancer cell death in the context of metabolic stress (32). PPARγ is a transcription factor capable of promoting pleiotropic effects, including the control of cell proliferation. Pharmacological agonists of PPARγ were used in cancer therapy with the aim of promoting cell cycle deceleration (33). TFP as AMPK inhibitor and PPARγ agonist facilitated to control tumor growth, which was confirmed by our present studies.

Finally, the cell cycle arrest of B16 cells treated with TFP could be due to both the inhibition of *de novo* fatty acid synthesis (causing inhibition of SREBP1) as well as the accumulation of exogeneous lipids in the nucleus (causing induction of PPARγ and impairment of cell proliferation through chromosome segregation abnormalities).

The present findings indicated that TFP activated lipid metabolism and the immune system. A balance between lipogenesis, lipid uptake and intracellular lipolysis is required to maintain lipid homeostasis (34). Cancer-associated adipocytes have been found to promote lipid accumulation (35). In the case of malignant melanoma, the tumor secreted an inhibitor of adipose LPL termed melanoma cachexia factor, which caused the inhibition of extracellular lipolysis (36). Activation of the transmembrane channel for exogenous free fatty acid uptake

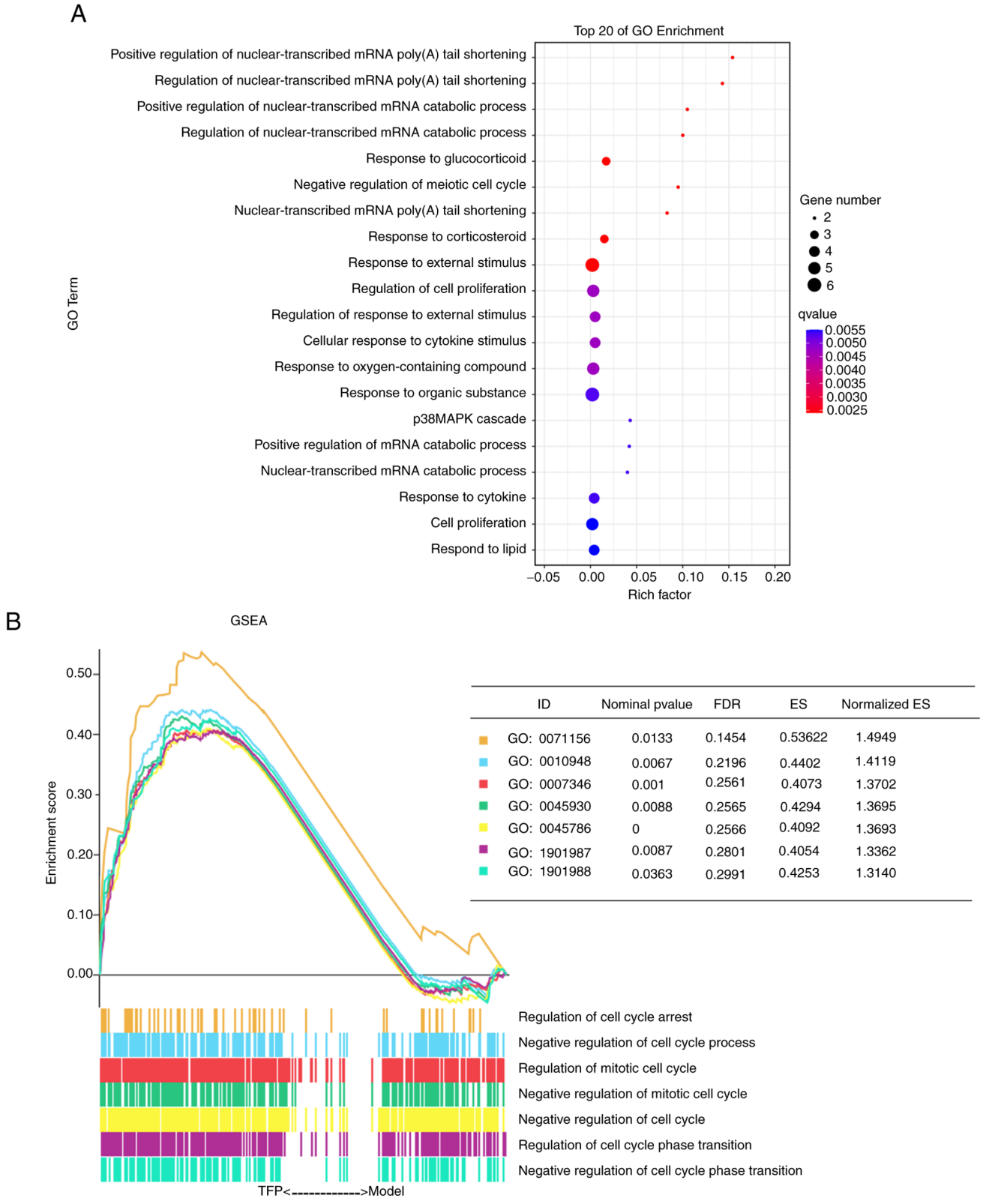

ID	Nominal pvalue	FDR	ES	Normalized ES
GO: 0071156	0.0133	0.1454	0.53622	1.4949
GO: 0010948	0.0067	0.2196	0.4402	1.4119
GO: 0007346	0.001	0.2561	0.4073	1.3702
GO: 0045930	0.0088	0.2565	0.4294	1.3695
GO: 0045786	0	0.2566	0.4092	1.3693
GO: 1901987	0.0087	0.2801	0.4054	1.3362
GO: 1901988	0.0363	0.2991	0.4253	1.3140

Figure 7. RNA-sequencing analysis confirms the effect of TFP on cell cycle. (A) Top 20 results of the GO pathway enrichment based on the DEGs identified in TFP-treated B16 allograft. In the scatter plot, the RichFactor corresponds to the ratio of the number of DEGs noted in a pathway term to all the genes noted in such pathway term, and a greater RichFactor means greater intensity. The Q-value is the corrected P-value ranging from 0 to 1, and a lower Q-value represents greater intensity. (B) GSEA revealed that cell cycle-related genes were significantly regulated. TFP, *Tremella fuciformis*-derived polysaccharide; GO, Gene Ontology; DEGs, differentially expressed genes; GSEA, Gene set enrichment analysis.

(CD36) and LPL (a key enzyme for extracellular lipolysis) confirmed the disposition of extracellular lipid stores and lipolysis in cells. The levels of free fatty acids, monoacylglycerides and diacylglycerides were not significantly elevated (data not shown), which suggested that lipid metabolism existed in cancer cells and cancer-associated adipocytes.

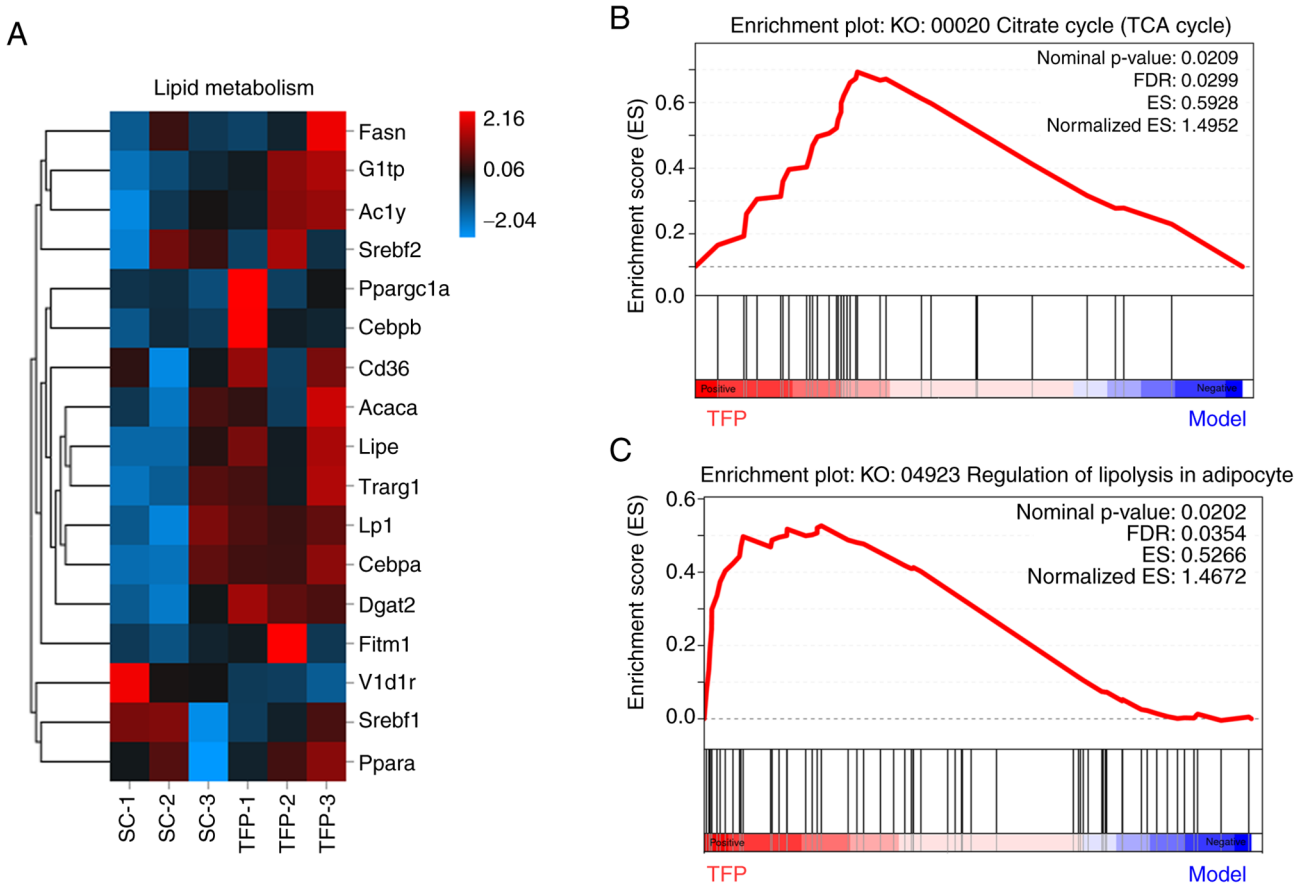

Figure 8. RNA-sequencing analysis confirms the effect of TFP on lipid metabolism. (A) Heatmap representation of differentially expressed genes associated with lipid metabolism in tumors treated with TFP. (B) Gene set enrichment analysis of the RNA-seq data was used to identify enriched biological pathway 'TCA cycle'. (C) Gene set enrichment analysis of the RNA-seq data was used to identify enriched biological pathway 'regulation of lipolysis in adipocyte'. TFP, *Tremella fuciformis*-derived polysaccharide.

Elevated SREBP1 in cancer cells increased *de novo* lipogenic gene expression, enhanced fatty acid synthesis, and accelerated triglyceride accumulation; however, these metabolic abnormalities were reversed by the treatment of B16 cells with TFP. TFP inhibited SREBP1 and AMPK, an enzyme that inhibits lipid synthesis through the phosphorylation and inactivation of key lipogenic enzymes. The net effect on lipogenic metabolism depends on a balance between opposing effects. In the present study, the net result was a decrease in SREBP1 and AMPK, while certain lipid enzymes were reduced (FAS and ACC) and certain others activated, particularly those participating in the tricarboxylic acid (TCA) cycle. Importantly, several signaling molecules involved in the processes of immune cell activation and transformation are derived from metabolites of the TCA cycle (37). These results indicated the crucial role of lipid metabolism in the regulation of the tumor immune microenvironment and the feasibility of targeting lipid metabolism to regulate tumor immunity.

Increasing evidence indicated that aberrant *de novo* lipogenesis is being increasingly recognized as important feature of malignant transformation (38), by contrast, the majority of normal human tissues use exogenous lipids, while *de novo* fatty acid synthesis is generally suppressed (39). *De novo* lipogenesis also determines the sensitivity of cancer cells to oxidative stress-induced cell death, and *de novo* synthesis was the preferred mechanism for fatty acid acquisition over lipolysis or receptor-mediated endocytosis (40). Tumor cells do not solely rely on *de novo* lipogenesis, but also utilize exogenous fatty acids for generating lipids for proliferation. Thus, despite the dominant role of *de novo* lipogenesis, exogenous fatty acids may also play an important role in cancer pathogenesis (41).

After B16 cells were exposed to TFP, their lipid metabolism was altered. TFP treatment resulted in the downregulation of *de novo* fatty acid synthesis due to feedback suppression with concomitant increase in exogenous fatty acid uptake. This metabolic change was facilitated by the upregulation of several key transporters, enzymes and signaling pathways. Specifically, CD36 and GLUT4 were remarkably upregulated; *de novo* lipogenesis was completely abolished; the lipid distribution in the cytoplasm was rearranged; and the lipid content in the cell membrane, ER and nucleus was elevated, which was accompanied by an increase in ACLY and PPARγ expression. The RNA-seq data precisely depicted the effect of TFP on lipid metabolism and processing, showing its antitumor effects. TFP caused excess lipid metabolism and dysregulated lipid storage in B16 cells, which resulted in the irreversible disruption of cell volume homeostasis and activation of the immune system.

There were a number of limitations to the present study. Firstly, functional experiments to demonstrate the effect of TFP in differentiated adipocytes should be performed to

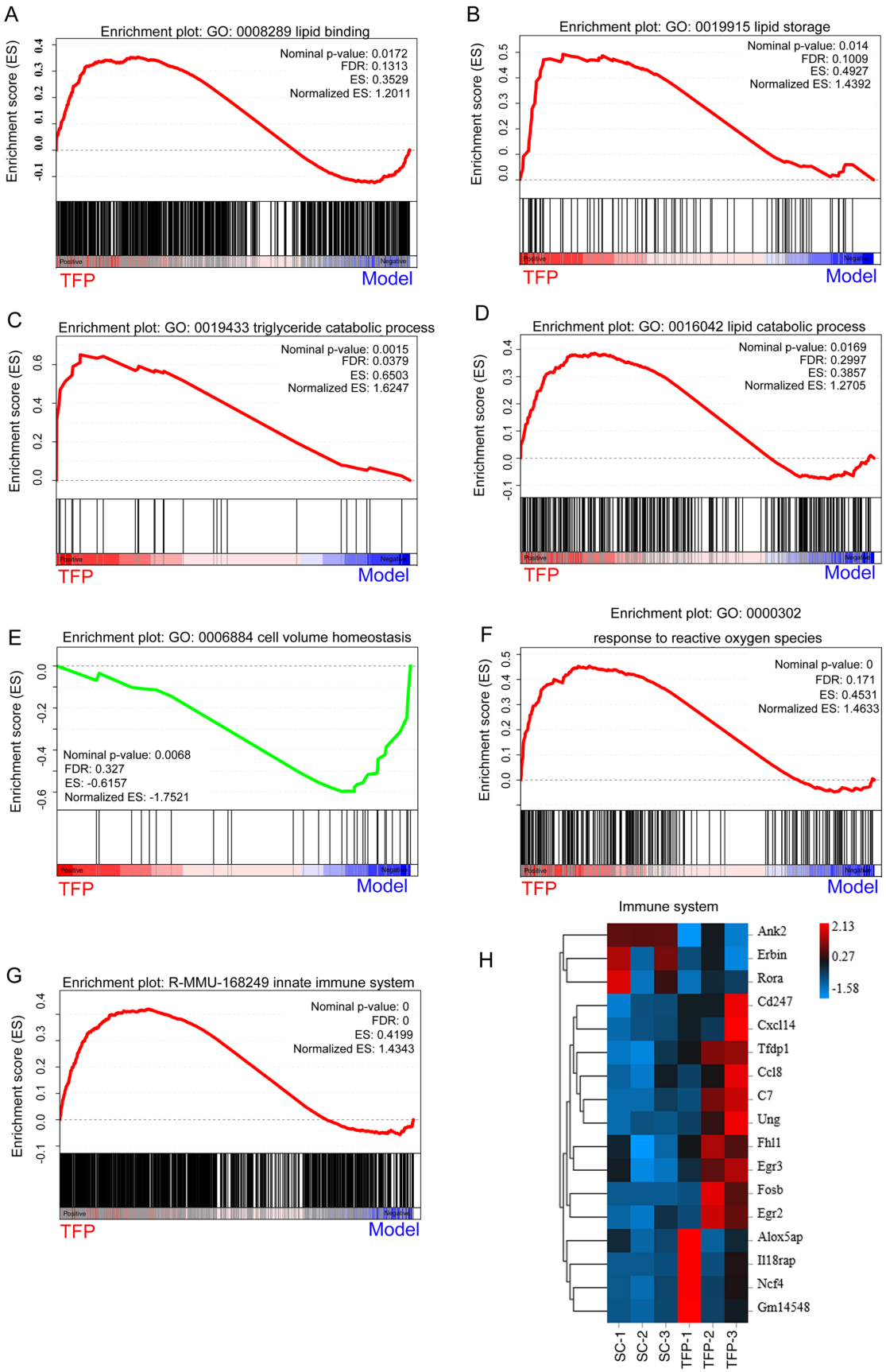

Figure 9. RNA-sequencing analysis confirms the mechanism of TFP on lipid metabolism and the immune system. Gene set enrichment analysis identified (A) positively enriched lipid binding, (B) lipid storage, (C) triglyceride, (D) lipid catabolic process, (E) cell volume homeostasis, (F) response to reactive oxygen species and (G) innate immune system. Heatmap representation of differentially expressed genes associated with immune response in tumors treated with TFP. (H) The vertical black lines indicated the position of each gene in the studied gene set. The normalized enrichment score and false discovery rate values are shown for each pathway. Heatmap representation of differentially expressed genes associated with the immune system in tumors. TFP, *Tremella fuciformis*-derived polysaccharide.

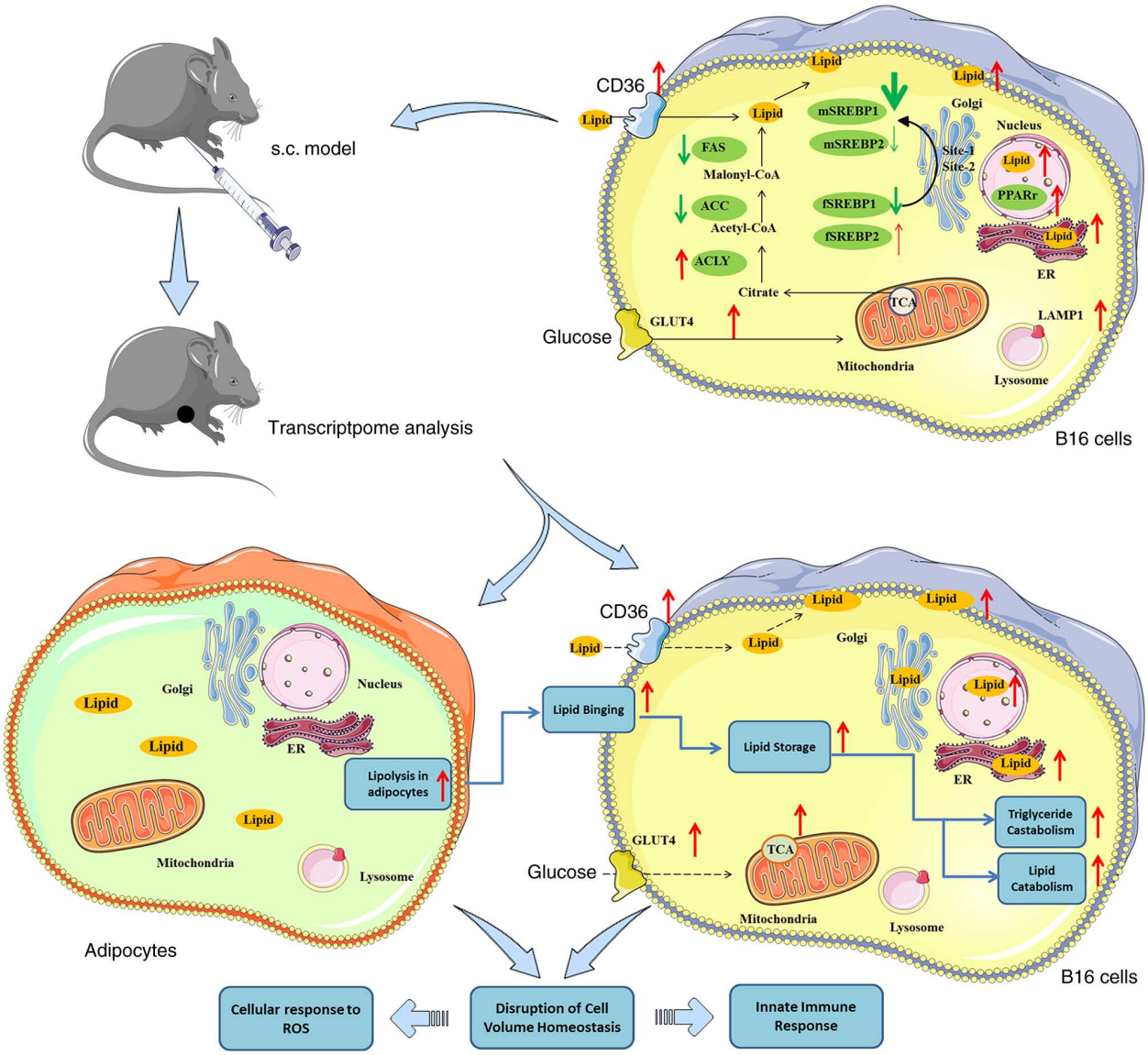

Figure 10. Scheme showing the potential mechanism of action of TFP, including lipid changes *in vitro* and transcriptional prolife *in vivo*. TFP inhibited *de novo* lipogenesis through downregulation of sterol regulatory element-binding transcription factor 1 while inducing the presence of lipids in the cytoplasm of B16 cells. This apparent contradiction was resolved by transcriptomic analysis *in vivo*, which revealed that the lipolysis of adipocytes supplied the lipids for B16 cells, which enhanced lipid binding, storage and catabolism. Overcharged lipid mechanisms depleted B16 cells and induced cell volume homeostasis disruption, thus activating the cellular response to reactive oxygen species and the innate immune response. TFP, *Tremella fuciformis* -derived polysaccharide.

demonstrate a specific role in TFP augmenting lipolysis of adipocytes. Secondly, mechanism of interactions between adipocytes and B16 cells should be explored. Thirdly, tumor cells manipulated *ex vivo* may serve as a uniquely effective carriers for the therapeutic delivery of bioactive cytokines to parental tumor by their homing properties especially highly metastatic cells (42). It is rarely reported that tumor cells modified with polysaccharides are used to treat tumors. The following antitumor effect and mechanism of B16 cells reprogrammed by TFP in vein in lower dosage was urgently needed in B16 subcutaneously implanted mice.

In conclusion, the present study identified the function of TFP on B16 cells, along with its unexpected molecular mechanism of action responsible for its antitumor effects, as summarized in the schematic diagram of Fig. 10. TFP inhibited *de novo* lipogenesis, although a larger number of lipids were present in the cytoplasm of B16 cells. TPF caused upregulated lipid binding, storage and catabolism with cellular response to reactive oxygen species, thus activating the immune system via disruption of cell volume homeostasis.

Acknowledgements

The authors would like to thank Dr Qici Wu and Bo Leng (The Engineering Technological Center of Mushroom Industry, Minnan Normal University, Zhangzhou, Fujian 363000, P.R. China). In the process of HPLC analysis of TFP in the present study, they provided numerous academic and constructive advices, and contributed to manuscript editing.

Funding

The present study was supported by the Natural Science fund in Fujian Province (grant no. 2021J011012), the Science and

Technology project of Zhangzhou city in Fujian Province (grant no. zz2021J44), the Scientific Research and Nurturing Projects of Minnan Normal University (grant no. MSPY2021) and the Records of National Science and Technology Projects (grant no. 2021L3027).

Availability of data and materials

The datasets used and/or analyzed during the current study are available from the corresponding author on reasonable request.

Authors' contributions

XL and YP conceived and designed the study. QS and XL performed the experiments. XL analyzed the data and wrote the manuscript. XL and YP confirm the authenticity of all the raw data. All authors read and approved the final version of the manuscript.

Ethics approval and consent to participate

The present study was approved (approval no. 2020002) and supervised by Experimental research Ethics Committee of Minna Normal University (Zhangzhou, China). All animal experiments were performed according to the relevant regulatory standards and were performed in accordance with the Experimental animal research Ethics Committee of Minna Normal University.

Patient consent for publication

Not applicable.

Competing interests

The authors declare that they have no competing interests.

References

1. Mizuta K, Matsubara T, Goto A, Addison WN, Nakatomi M, Matsuo K, Tada-Shigeyama Y, Yaginuma T, Honda H, Yoshioka I and Kokabu S: Plectin promotes tumor formation by B16 mouse melanoma cells via regulation of Rous sarcoma oncogene activity. BMC Cancer 22: 936, 2022.
2. Wang E, Liu Y, Xu C and Liu J: Antiproliferative and proapoptotic activities of anthocyanin and anthocyanidin extracts from blueberry fruits on B16-F10 melanoma cells. Food Nutr Res 61: 1325308, 2017.
3. Emens LA, Ascierto PA, Darcy PK, Demaria S, Eggermont AMM, Redmond WL, Seliger B and Marincola FM: Cancer immunotherapy: Opportunities and challenges in the rapidly evolving clinical landscape. Eur J Cancer 81: 116-129, 2017.
4. Navarro C, Ortega A, Santeliz R, Garrido B, Chacín M, Galban N, Vera I, De Sanctis JB and Bermúdez V: Metabolic reprogramming in cancer cells: Emerging molecular mechanisms and novel therapeutic approaches. Pharmaceutics 14: 1303, 2022.
5. Zhao Q, Lin X and Wang G: Targeting SREBP-1-mediated lipogenesis as potential strategies for cancer. Front Oncol 12: 952371, 2022.
6. Li J, Shen H, Owens GK and Guo LW: SREBP1 regulates Lgals3 activation in response to cholesterol loading. Mol Ther Nucleic Acids 28: 892-909, 2022.
7. Bindesboll C, Aas A, Ogmundsdottir MH, Pankiv S, Reine T, Zoncu R and Simonsen A: NBEAL1 controls SREBP2 processing and cholesterol metabolism and is a susceptibility locus for coronary artery disease. Sci Rep 10: 4528, 2020.
8. Luo H, Chen CY, Li X, Zhang X, Su CW, Liu Y, Cao T, Hao L, Wang M and Kang JX: Increased lipogenesis is critical for self-renewal and growth of breast cancer stem cells: Impact of omega-3 fatty acids. Stem Cells 39: 1660-1670, 2021.
9. Kitamura K, Erlangga JS, Tsukamoto S, Sakamoto Y, Mabashi-Asazuma H and Iida K: Daidzein promotes the expression of oxidative phosphorylation- and fatty acid oxidation-related genes via an estrogen-related receptor alpha pathway to decrease lipid accumulation in muscle cells. J Nutr Biochem 77: 108315, 2020.
10. Hu B, Lin JZ, Yang XB and Sang XT: Aberrant lipid metabolism in hepatocellular carcinoma cells as well as immune microenvironment: A review. Cell Prolif 53: e12772, 2020.
11. Simeone P, Tacconi S, Longo S, Lanuti P, Bravaccini S, Pirini F, Ravaioli S, Dini L and Giudetti AM: Expanding roles of de novo lipogenesis in breast cancer. Int J Environ Res Public Health 18: 3575, 2021.
12. Zhao S, Torres A, Henry RA, Trefely S, Wallace M, Lee JV, Carrer A, Sengupta A, Campbell SL, Kuo YM, *et al*: ATP-citrate lyase controls a glucose-to-acetate metabolic switch. Cell Rep 17: 1037-1052, 2016.
13. Ramapriyan R, Caetano MS, Barsoumian HB, Mafra ACP, Zambalde EP, Menon H, Tsouko E, Welsh JW and Cortez MA: Altered cancer metabolism in mechanisms of immunotherapy resistance. Pharmacol Ther 195: 162-171, 2019.
14. Welte MA: Expanding roles for lipid droplets. Curr Biol 25: R470-R481, 2015.
15. Todisco S, Santarsiero A, Convertini P, De Stefano G, Gilio M, Iacobazzi V and Infantino V: PPAR alpha as a metabolic modulator of the liver: Role in the pathogenesis of nonalcoholic steatohepatitis (NASH). Biology (Basel) 11: 792, 2022.
16. Thiam AR, Farese RV Jr and Walther TC: The biophysics and cell biology of lipid droplets. Nat Rev Mol Cell Biol 14: 775-786, 2013.
17. Hashemi HF and Goodman JM: The life cycle of lipid droplets. Curr Opin Cell Biol 33: 119-124, 2015.
18. Cartwright BR, Binns DD, Hilton CL, Han S, Gao Q and Goodman JM: Seipin performs dissectible functions in promoting lipid droplet biogenesis and regulating droplet morphology. Mol Biol Cell 26: 726-739, 2015.
19. Shen T, Duan C, Chen B, Li M, Ruan Y, Xu D, Shi D, Yu D, Li J and Wang C: Tremella fuciformis polysaccharide suppresses hydrogen peroxide-triggered injury of human skin fibroblasts via upregulation of SIRT1. Mol Med Rep 16: 1340-1346, 2017.
20. Terrazas C, Oghumu S, Varikuti S, Martinez-Saucedo D, Beverley SM and Satoskar AR: Uncovering Leishmania-macrophage interplay using imaging flow cytometry. J Immunol Methods 423: 93-98, 2015.
21. Lee YT, Lim SH, Lee B, Kang I and Yeo EJ: Compound C Inhibits B16-F1 tumor growth in a syngeneic mouse model via the blockage of cell cycle progression and angiogenesis. Cancers (Basel) 11: 823, 2019.
22. Subramanian A, Tamayo P, Mootha VK, Mukherjee S, Ebert BL, Gillette MA, Paulovich A, Pomeroy SL, Golub TR, Lander ES and Mesirov JP: Gene set enrichment analysis: A knowledge-based approach for interpreting genome-wide expression profiles. Proc Natl Acad Sci USA 102: 15545-15550, 2005.
23. Steinbusch LK, Schwenk RW, Ouwens DM, Diamant M, Glatz JF and Luiken JJ: Subcellular trafficking of the substrate transporters GLUT4 and CD36 in cardiomyocytes. Cell Mol Life Sci 68: 2525-2538, 2011.
24. Romanauska A and Kohler A: The inner nuclear membrane is a metabolically active territory that generates nuclear lipid droplets. Cell 174: 700-715 e718, 2018.
25. Chiu CH, Chiu KC and Yang LC: Amelioration of obesity in mice fed a high-fat diet with uronic acid-rich polysaccharides derived from tremella fuciformis. Polymers (Basel) 14: 1514, 2022.
26. Shao W and Espenshade PJ: Expanding roles for SREBP in metabolism. Cell Metab 16: 414-419, 2012.
27. Guo D, Bell EH, Mischel P and Chakravarti A: Targeting SREBP-1-driven lipid metabolism to treat cancer. Curr Pharm Des 20: 2619-2626, 2014.
28. Queiroz EA, Fortes ZB, da Cunha MA, Barbosa AM, Khaper N and Dekker RF: Antiproliferative and pro-apoptotic effects of three fungal exocellular beta-glucans in MCF-7 breast cancer cells is mediated by oxidative stress, AMP-activated protein kinase (AMPK) and the Forkhead transcription factor, FOXO3a. Int J Biochem Cell Biol 67: 14-24, 2015.
29. Kim I and He YY: Targeting the AMP-activated protein kinase for cancer prevention and therapy. Front Oncol 3: 175, 2013.

30. Li Y, Xu S, Mihaylova MM, Zheng B, Hou X, Jiang B, Park O, Luo Z, Lefai E, Shyy JYJ, *et al*: AMPK phosphorylates and inhibits SREBP activity to attenuate hepatic steatosis and atherosclerosis in diet-induced insulin-resistant mice. Cell Metab 13: 376-388, 2011.
31. Rigel J, Kishton, Carson E, Cohen S, Gerriets VA, Siska PJ, Macintyre AN, Goraksha-Hicks P, de Cubas AA, Liu T, *et al*: AMPK is essential to balance glycolysis and mitochondrial metabolism to control T-ALL cell stress and survival. Cell Metab 12: 649-662, 2016.
32. Jeon SM, Chandel NS and Hay N: AMPK regulates NADPH homeostasis to promote tumour cell survival during energy stress. Nature 485: 661-665, 2012.
33. Flori E, Rosati E, Cardinali G, Kovacs D, Bellei B, Picardo M and Maresca V: The α-melanocyte stimulating hormone/peroxisome proliferator activated receptor-γ pathway down-regulates proliferation in melanoma cell lines. J Exp Clin Cancer Res 36: 142, 2017.
34. Cheng C, Geng F, Cheng X and Guo D: Lipid metabolism reprogramming and its potential targets in cancer. Cancer Commun (Lond) 38: 27, 2018.
35. Wu Q, Li B, Li Z, Li J, Sun S and Sun S: Cancer-associated adipocytes: Key players in breast cancer progression. J Hematol Oncol 12: 95, 2019.
36. Martin P: Cancer cachexia syndrome: Reflecting on 20 years of providing cancer cachexia care as the leader of an interdisciplinary team in an Australian cancer center. Asia Pac J Oncol Nurs 9: 100070, 2022.
37. Ryan DG, Murphy MP, Frezza C, Prag HA, Chouchani ET, O'Neill LA and Mills EL: Coupling Krebs cycle metabolites to signalling in immunity and cancer. Nat Metab 1: 16-33, 2019.
38. Bartolacci C, Andreani C, Vale G, Berto S, Melegari M, Crouch AC, Baluya DL, Kemble G, Hodges K, Starrett J, *et al*: Targeting de novo lipogenesis and the Lands cycle induces ferroptosis in KRAS-mutant lung cancer. Nat Commun 13: 4327, 2022.
39. Li L, Che L, Tharp KM, Park HM, Pilo MG, Cao D, Cigliano A, Latte G, Xu Z, Ribback S, *et al*: Differential requirement for de novo lipogenesis in cholangiocarcinoma and hepatocellular carcinoma of mice and humans. Hepatology 63: 1900-1913, 2016.
40. Zaidi N, Lupien L, Kuemmerle NB, Kinlaw WB, Swinnen JV and Smans K: Lipogenesis and lipolysis: The pathways exploited by the cancer cells to acquire fatty acids. Prog Lipid Res 52: 585-589, 2013.
41. Rizzo AM, Colombo I, Montorfano G, Zava S and Corsetto PA: Exogenous fatty acids modulate ER lipid composition and metabolism in breast cancer cells. Cells 10: 175, 2021.
42. Dondossola E, Dobroff AS, Marchio S, Cardó-Vila M, Hosoya H, Libutti SK, Corti A, Sidman RL, Arap W and Pasqualini R: Self-targeting of TNF-releasing cancer cells in preclinical models of primary and metastatic tumors. Proc Natl Acad Sci USA 113: 2223-2228, 2016.